electronics

MDPI

Article

A Novel Distribution Network Reconfiguration Method with the Power Forecasting of DGs

Wangli Feng [1,2,3,*], Lei Su [1,2,3], Cao Kan [1,2,3], Mingjiang Wei [1,2,3], Ruoshi Gu [1,2,3] and Xiaomeng Yang [4]

[1] State Grid Hubei Electric Power Research Institute, Wuhan 430077, China; sulei@icloud.com (L.S.); caok@hb.sgcc.com.cn (C.K.); weimj@hb.sgcc.com.cn (M.W.); ruoshigu1999@163.com (R.G.)
[2] Hubei Key Laboratory of Regional New Power Systems and Rural Energy System Configuration, Wuhan 430077, China
[3] Hubei Engineering Research Center of the Construction and Operation Control Technology of New Power Systems, Wuhan 430077, China
[4] School of Electrical and Information Engineering, Yuntang Campus, Changsha University of Science & Technology, Changsha 410114, China
* Correspondence: fwl62313@163.com

Abstract

As the development and utilization of renewable energy increase, more distributed generators (DGs) are employed in distribution systems. When a line fault occurs, the inherent intermittency and randomness of DGs' power are a challenge for distribution network reconfiguration. In this paper, to reduce the influence of power uncertainty, a novel fault reconfiguration method is proposed with the power forecasting of DGs. First, a hybrid power forecasting method is proposed to predict the short-term power of DGs. The history power data of DGs are decomposed by the VMD method, and the decomposition signals are inputted into the TCN-LSTM method. The learning factor and penalty coefficient of TCN-LSTM are optimized by the sparrow search algorithm (SSA) to acquire better prediction results. Then, according to the prediction values of DGs, a fault reconfiguration method is constructed with maximum power restoration and minimum network losses, where the switch operation counts and island operation are taken into account. Simulation results verify the effectiveness of the proposed method. The VMD-SSA-TCN-LSTM method has a better performance than traditional forecasting methods in short-term prediction. The proposed fault reconfiguration method can restore the non-fault line load effectively and is suitable for multi-line fault conditions.

Keywords: fault reconfiguration; power forecasting; TCN-LSTM; sparrow search algorithm

Check for updates

Academic Editor: Fabio Corti

Received: 5 August 2026
Revised: 25 September 2026
Accepted: 29 September 2026
Published: 9 October 2026

Copyright: © 2026 by the authors. Licensee MDPI, Basel, Switzerland. This article is an open access article distributed under the terms and conditions of the Creative Commons Attribution (CC BY) license.

1. Introduction

A distribution network plays an indispensable role in ensuring power supply, promoting economic development, and improving public services. The failures directly impact societal production and residents' daily power supply. Distribution network reconfiguration is a method for rapid restoration, which can redistribute power flow, enabling swift restoration of supply to unaffected areas by altering switch states on lines [1]. With the widespread integration of distributed renewable energy into distribution grids, the economic efficiency and flexibility of distribution networks have been significantly enhanced. However, the inherent uncertainties in renewable energy output and other limitations also impose new demands on distribution network fault reconstruction [1,2].

Traditional fault reconfiguration methods primarily rely on static restoration, which mainly performs calculations based on the system operating state at the time of the fault.

However, they ignore the impact of the dynamic variation in renewable energy output over time [3]. The uncertainty of renewable energy output affects the power balance and power quality of distribution networks [4]. To ensure the long-term stable operation of the restored system, fault reconfiguration methods must consider multi-period changes in source and load power [5].

Regarding fault restoration in distribution networks incorporating distributed renewable energy, extensive research has been conducted globally. Ref. [6] analyzes the impact of intermittent and uncertain renewable generation on system stability, proposing a probabilistic load flow fault restoration method based on voltage sensitivity. In [7], the authors introduce a typical load time-varying demand model to establish a fault restoration framework, demonstrating that incorporating long-term load power variations effectively enhances fault recovery performance. References [8,9] address the time-varying nature of sources and loads by proposing a dynamic reconstruction method based on source-load forecasts that balances network losses, outage load quantities, and power quality. Regarding uncertainty in source-load factors, [10] employs Monte Carlo scenario generation, selects representative samples via k-means clustering, and then performs optimization based on these. In contrast, [11] quantifies uncertainty using conditional value-at-risk theory, converting its impact into risk costs and integrating these into the objective function of the reconstruction algorithm.

In order to reduce the influence of the uncertainty of DGs, accurate and reliable forecasting methods for PV power generation can assist grid operators in effectively managing the variability and uncertainty of renewable energy affected by weather and other factors, improving grid stability and renewable energy integration efficiency [12].

Forecasting methods are typically categorized into physical forecasting methods and statistical forecasting methods [13,14]. Physical forecasting methods establish prediction models based on power generation principles, but they demand excessive model accuracy and are prone to bias [15]. Statistical forecasting methods achieve photovoltaic power prediction by establishing mapping relationships between data, offering advantages of high efficiency and accuracy [16]. Statistical methods include support vector machines [17], extreme learning machines [18], and artificial neural networks [19].

Machine learning technologies can automatically learn input features from historical data. Long Short-Term Memory (LSTM) networks are neural network models designed for sequence data prediction, effectively enhancing the accuracy of photovoltaic power forecasting by uncovering the temporal characteristics of input meteorological features. In [20,21], the authors proposed a regional distributed PV power forecasting model based on Long Short-Term Memory Networks (LSTNet), which combines the long-term and short-term spatiotemporal characteristics of PV power and meteorological factor sequences, thereby improving prediction accuracy and robustness.

Ref. [22] employed Long Short-Term Memory (LSTM) algorithms to forecast generation at a Brazilian PV plant, achieving significantly higher prediction accuracy than Backpropagation Neural Network (BPNN) models. Reference [23] extracts meteorological factor features and performs dimensionality reduction, proposing a hybrid photovoltaic power prediction model based on BiLSTM. By utilizing an improved particle swarm optimization algorithm to optimize the inertia weight of the inverse sine function, the predictive performance of the hybrid photovoltaic model is enhanced. LSTM networks only reflect the data characteristics of time series, with insufficient spatial distribution prediction capabilities. Combined prediction models can improve the predictive performance of LSTM-based network models. The TCN-LSTM model is adopted in this paper to exploit both the temporal feature extraction capability of a TCN and the sequential modeling ability of LSTM for short-term PV power forecasting.

In recent years, metaheuristic optimization algorithms have been increasingly employed in photovoltaic power forecasting to reduce the dependence of forecasting models on manual parameter tuning. In [24], PSO was employed to optimize the hyperparameters of the LSTM network and determine an appropriate network structure for short-term PV power forecasting. In [25], WOA was introduced to optimize the key parameters of VMD, thereby reducing the influence of empirical parameter selection on the decomposition performance of PV power sequences. In this paper, the sparrow search algorithm (SSA) [26] is employed to optimize the key parameters of the TCN-LSTM model.

Therefore, this paper proposes a fault recovery method based on a chaotic binary sparrow search algorithm for active distribution networks. A fault reconfiguration method is proposed with the power forecasting of DGs. First, a hybrid power forecasting method is proposed to predict the short-term power of DGs. The history power data of DGs are decomposed by the VMD method, and the decomposition signals are inputted into the TCN-LSTM method. The learning factor and penalty coefficient of TCN-LSTM are optimized by the sparrow search algorithm (SSA) to acquire better prediction results. Then, according to the prediction values of DGs, a fault reconfiguration method is constructed with maximum power restoration and minimum network losses, where the switch operation counts and island operation are taken into account. Simulation results verify the effectiveness of the proposed method. The VMD-SSA-TCN-LSTM method has a better performance than traditional forecasting methods in short-term prediction. The proposed fault reconfiguration method can restore the non-fault line load effectively and is suitable for multi-line fault conditions.

2. Forecasting Methods

Accurate short-term PV power forecasting can provide reliable information for the operation and service restoration of distribution networks with distributed photovoltaic generation. Owing to the intermittency and variability of PV output, the original power sequence is decomposed into several sub-sequences to reduce forecasting complexity and improve prediction accuracy. Among existing signal decomposition techniques, EMD is widely used. However, the number of IMF components in EMD cannot be arbitrarily set, and modal confusion often occurs during decomposition. VMD addresses both these shortcomings; hence, this paper employs VMD for decomposing power data.

2.1. VMD Method

The Variational Modal Decomposition (VMD) method is an estimation technique that decomposes dynamic non-stationary parametric signals under specific constraints. It possesses the capability to simultaneously process both recursive and non-recursive signals, enabling the decomposition of complex original signals. Particularly when handling non-stationary and nonlinear time series, the VMD method significantly optimizes the endpoint effects and decomposed modes of EMD.

The specific steps are as follows:

(1) Solving the Constructed Variational Problem

The constructed variational problem is formulated with the constraint that the sum of all modal components equals the original signal:

$$\begin{aligned} &\min_{\{u_k\},\{\omega_k\}} \left\{ \sum_k \left\| \partial_t \left[(\delta(t) + \frac{j}{\pi t}) * u_k(t) \right] e^{-j\omega_k t} \right\|_2^2 \right\} \\ &s.t. \quad \sum_{k=1}^{K} u_k = f(t) \end{aligned} \tag{1}$$

where K is the number of decomposed modes; $\{u_k\}$ is the kth modal component obtained from decomposition; $\{\omega_k\}$ is the center frequency; $*$ is the convolution operation; $f(t)$ is the original signal; ∂_t is the gradient operation.

(2) Solving Constrained Variational Problems

To solve Equation (1), introduce the Lagrange multiplier operator and a quadratic penalty factor α. The objective is to transform the constrained variational problem into an unconstrained variational problem to mitigate Gaussian noise interference. The Alternating Direction Method of Multipliers (ADMM) [26] continuously updates each component and the central frequency to obtain the optimal solution to the unconstrained problem. The expression is shown as

$$\begin{aligned} L(\{p_k\},\{\omega_k\},\lambda(t)) &= \alpha\sum_k \left\| \partial_t[\left(\delta(t)+\frac{j}{\pi t}\right) * p_k(t)]e^{-j\omega t} \right\|_2^2 \\ &+ \left\| f(t)-\sum_k p_k(t) \right\|_2^2 + \left[\lambda(t), f(t)-\sum_k p_k(t)\right] \end{aligned} \tag{2}$$

In the equation, α—quadratic penalty parameter; λ—Lagrange multiplier.

2.2. SSA Method

The sparrow search algorithm (SSA) [26] is a population-based metaheuristic optimization algorithm inspired by the foraging and anti-predation behavior of sparrows. In SSA, individuals are categorized into three types: explorers, followers, and sentinels. Each individual's position corresponds to a solution. The algorithm iteratively updates the positions of these three types of individuals, calculating the fitness values of all individuals at each iteration to determine the optimal solution's position.

The main update and iteration steps are as follows:

(1) Explorer Location Update

The explorers check for predators within the foraging area. During each iteration, the explorer's position is updated according to the following formula:

$$X_{i,j}^{t+1} = \begin{cases} X_{i,j}^t \cdot \exp(\frac{-i}{\alpha \cdot t_{\max}}), R < S_T \\ X_{i,j}^t + QL, R \geq S_T \end{cases} \tag{3}$$

where t denotes the total number of iterations; t_{max} denotes the maximum number of iterations; i and j denote the i-th sparrow and the j-th dimension at the current iteration; $X_{i,j}^t$ denotes the position of a sparrow individual in a certain dimension; $\alpha \in (0, 1]$ denotes a random number; R and S_T denote the warning threshold and safety threshold, with threshold ranges [0, 1] and [0.5, 1], respectively; Q is a random number following a normal distribution; L is a $1 \times d$ matrix where all variables are set to 1.

(2) Follower Location Update

When a follower joins, determine whether it qualifies to compete for food with the discoverer—that is, whether its position is more advantageous. If the fitness corresponding to its position is lower, it is ineligible to compete and must fly to another area to forage. Otherwise, the newcomer will forage near the optimal individual X_P. The expression is as follows:

$$X_i^{t+1} = \begin{cases} Q \cdot \exp(\frac{X_W^t - X_i^t}{t^2}), i < \frac{n}{2} \\ X_P^{t+1} + \left| X_i^t - X_P^{t+1} \right| A^+ L, i \geq \frac{n}{2} \end{cases} \tag{4}$$

where X_w denotes the position of the individual with the worst fitness in generation t; X_P represents the position of the individual with the best fitness in generation t + 1; i > n/2

indicates that the i-th follower cannot obtain food by following the discoverer and must therefore fly elsewhere to forage; $\boldsymbol{A}$ is a row vector with the same dimensions as L^{T}, whose elements are randomly initialized as 1 or -1, satisfying $\boldsymbol{A}^{+} = \boldsymbol{A}^{\mathrm{T}}(\boldsymbol{A}\boldsymbol{A}^{\mathrm{T}})^{-1}$.

(3) Sentinel Location Update

Within the population, some sparrows remain constantly vigilant for nearby dangers while foraging. Upon detecting a threat, they abandon their food or foraging activity and fly to a safe area to resume foraging. In each generation of the population, n sparrows are assigned to serve as sentinels. Their position update formula is

$$X_{i,j}^{t+1} = \begin{cases} X_b^{t+1} + \beta(X_{i,j}^t - X_b^t), f_t \neq f_g \\ X_{i,j}^t + u(\frac{X_{i,j}^t - X_w^t}{|f_t - f_w| + \varepsilon}), f_t = f_g \end{cases} \quad (5)$$

where β is a random number conforming to the standard normal distribution; X_b is the current global optimal position; f_i is the current sparrow fitness value; f_g is the current fitness value; f_w is the worst fitness value; I is the uniform random number in $[-1, 1]$; ε is the small number to prevent a zero denominator; $X_{i,j}^{t+1}$ is the position of sentinel j in iteration $t + 1$.

2.3. TCN Method

Compared to other convolutional neural networks (CNNs), the Temporal Convolutional Network (TCN) inherits powerful feature extraction capabilities and is particularly adept at processing time-series data [27].

It introduces causal convolutions and dilated convolutions, enabling the TCN to better capture temporal relationships when processing sequences. Furthermore, the TCN incorporates residual connections between each layer of the network, which not only aids in extracting sequence features but also cleverly avoids the vanishing and exploding gradient problems commonly encountered when training deep networks [27].

(1) Causal Convolution

Causal convolution is a special one-dimensional convolutional structure. Since the data being processed is a time series, the convolutional output at time step t + 1 depends only on the current time step t and previous inputs, thereby effectively capturing the temporal dependence of PV power sequences.

(2) Dilated Convolution

Dilated convolution is a key structure in a TCN, used to capture global feature data. Dilated convolutions introduce a dilation rate into the convolutional layers, expanding the receptive field by controlling the stride of the convolutional kernel along the temporal dimension, thereby enabling the capture of dependencies over longer time ranges. The calculation formula for dilated convolutions is shown as

$$F(s) = (x \cdot df)(s) = \sum_{i=0}^{k-1} f(i) X_{x-di} \quad (6)$$

(3) Residual Connections

In TCNs, residual connections are implemented by performing element-wise addition between a block's input and its output, thereby allowing information to flow directly from the block's input to its output, bypassing the convolutional layers within the block. It enables the network to learn residual mappings that capture incremental changes in the input data, which helps mitigate the vanishing gradient problem and improves information

flow within the network. The TCN residual block structure is built by combining the causal convolutions, dilated convolutions, and residual connections.

2.4. Long Short-Term Memory Method

A Long Short-Term Memory (LSTM) network is a specialized neural network model, which incorporates a unit state structure beyond conventional neural networks to effectively address issues such as vanishing or exploding gradients in standard neural networks [22]. Each neuron can be represented as

$$\begin{aligned} f_t &= \sigma\left(W_f[h_{t-1}, x_t] + b_f\right) \\ i_t &= \sigma(W_i[h_{t-1}, x_t] + b_i) \\ \tilde{c}_t &= \tanh(W_c[h_{t-1}, x_t] + b_c) \\ c_t &= f_t \odot c_{t-1} + i_t \odot \tilde{c}_t \\ o_t &= \sigma(W_o[h_{t-1}, x_t] + b_o) \\ h_t &= o_t \odot \tan h(c_t) \end{aligned} \tag{7}$$

$$z_t = \begin{bmatrix} h_{t-1} \\ x_t \end{bmatrix} \tag{8}$$

where f_t, i_t, and o_t denote the forget gate, input gate, and output gate at time t, respectively; c_t denotes the cell state, and $\tilde{c}_t$ represents the candidate cell state; h_t denotes the hidden state; x_t is the input vector at time t; and z_t is the concatenated vector composed of the previous hidden state h_{t-1} and the current input x_t. W_f, W_i, W_c, and W_o are the corresponding weight matrices, while b_f, b_i, b_c, and b_o are the bias vectors. $\sigma(\cdot)$ and $\tanh(\cdot)$ denote the sigmoid and hyperbolic tangent activation functions, respectively, and $\odot$ represents element-wise multiplication.

Using SSA to optimize the learning factor and penalty coefficient of TCN-LSTM is simpler and more effective than traditional multi-frequency cross-validation methods. The specific steps are as follows:

(1) Preprocess the data and construct the TCN-LSTM model.
(2) Dynamically update multiple population parameters such as population size, iteration count, and explorer–exploiter ratio, and adjust the learning parameter range.
(3) Calibrate the fitness values of the sparrow search algorithm and dynamically adjust search strategies and parameter settings based on fitness value changes. Employing the SSA, use root mean square error (RMSE) as the objective function to identify the optimal fitness.
(4) Incorporate the optimal fitness value into the TCN-LSTM for a specified training proportion, yielding the optimized SSA-TCN-LSTM prediction model.
(5) Input the test samples into the optimized model to obtain the predicted PV power.

3. Reconfiguration Method for Distribution Network

3.1. Objective Function

After a fault occurs at the line of the distribution network, the primary objective of distribution network fault restoration is to restore as much load as possible. However, given the economic and network losses during post-recovery operation, voltage quality and the number of switching operations for recovery strategies must also be comprehensively considered. Therefore, the objective function is defined to restore power to more areas while minimizing network losses during post-recovery operation and switch operation counts:

$$\min T = c_d[\sum_{d \in S}(1 - Z_d) + \sum_{d \in M} Z_d] + c_l I_l^2 R_l + c_{load} S \tag{9}$$

The weighting coefficients used in the objective function are listed in Table 1. These coefficients are kept unchanged in all reconfiguration case studies to ensure a consistent comparison among different scenarios.

Table 1. Weighting coefficients used in the reconfiguration objective function.

Parameter	Description	Value
C_d	Weighting coefficient of switching operations	5
C_l	Weighting coefficient of network loss	1
C_{load}	Weighting coefficient of load shedding	10

3.2. Island Constraints

In the process of island partitioning, it is necessary to ensure that the loads with high restoration priority are recovered first, followed by restoring as many other loads as possible and shedding the minimum number of loads. Therefore, the objective function for island partitioning is as follows:

$$F = \sum_{i \in N} \delta_i P_i \beta_i \tag{10}$$

where N is the total number of nodes; P_i is the active power of node i; y_i is the power supply status of node i, which takes a value of 0 or 1, representing that the load is not restored or restored, respectively.

Considering the influence of loads' criticality, they are categorized into primary, secondary, and tertiary loads. For primary loads, power must be restored immediately upon failure. For other loads, the priority for restoration is determined based on their importance. Therefore, the priority restoration coefficients are as follows:

$$\delta_t = F_W P_i(t) \tag{11}$$

where N denotes all load nodes within the islanded system; ω_i represents the load-priority restoration coefficient for node i; P_i indicates the active-power magnitude at node i; y_i signifies the power supply status of node i at time t, where y_i = 0 indicates the load has not been restored and y_i = 1 indicates the load has been restored. Meanwhile, DG units within the distribution network are treated as combined power sources possessing black start capability.

3.3. Other Constraints

(1) Island Power constraints

$$\sum_{i=1}^{N} P_{r,t} \geq \sum_{i \in M} P_{i,t} + P_{loss,t} \tag{12}$$

where N and M are the number of DGs and the number of island nodes, respectively; P_r, t is the output of the r-th DG at time t; P_i, t is the active power of node i at time t; Ploss, t is the power loss at time t.

(2) Power Balance constraints

$$\begin{cases} P_i = U_i \sum\limits_{j=1}^{N} U_j (G_{ij} \cos\theta_{ij} + B_{ij} \sin\theta_{ij}) \\ Q_i = U_i \sum\limits_{j=1}^{N} U_j (G_{ij} \sin\theta_{ij} - B_{ij} \cos\theta_{ij}) \end{cases} \tag{13}$$

where P_i and Q_i are the active power and reactive power of node i, respectively; U_i is the voltage amplitude of node i; G_{ij} is the conductance between node i and node j; θ_{ij} is the voltage phase angle difference between node i and node j; B_{ij} is the susceptance between node i and node j.

(3) Capacity constraints

$$|P_l| \leq P_{l\max} \tag{14}$$

where P_l and P_{lmax} are the active power and maximum active power of branch l, respectively.

(4) Voltage constraints

$$U_{i\min} \leq U_i \leq U_{i\max} \tag{15}$$

where U_i is the voltage amplitude, U_{imin} is the minimum value of voltage amplitude, and U_{imax} is the maximum value of voltage amplitude.

(5) Network radial operation constraints

$$g \in G \tag{16}$$

where g denotes the restored normal area; G denotes the radial topological structure of the network.

3.4. Topological Search Methods

Utilize Breadth-First Search (BFS) and Depth-First Search (DFS) to traverse the distribution network topology during islanding partitioning. BFS begins at the root node, traversing connected nodes while numbering them. It then uses these nodes as vertices to search their child nodes in the next layer, repeating this process layer by layer until all nodes are explored. DFS begins at the root node. If an unexplored edge originating from this node is encountered, the search proceeds along that edge. Once all edges from a node have been traversed, the search backtracks to the starting point of the edge that led to that node. This process continues until all reachable nodes from the root are explored.

3.5. Topological Search Methods Using Island Partitioning Strategy

(1) Acquire the initial data of the active distribution network, including network topology, impedance, and loads.
(2) Calculate the output values of distributed generators and the priority restoration coefficients of loads at the fault moment.
(3) Conduct a circular search for the output values at the fault moment based on distributed generator nodes. Adopt the breadth-first traversal algorithm to determine the scope of the power output circle of distributed generators. If other distributed generators are included in the circle, it indicates the occurrence of island overlapping, and island combination shall then be implemented.
(4) Based on critical load nodes, adopt the depth-first traversal algorithm to incorporate these nodes into the nearest island.
(5) Judge whether the island power exceeds the limit. If the limit is exceeded, shed non-critical loads according to the priority restoration coefficients and reduce the island scope to make the island satisfy the power constraints. Finally, form the island partitioning strategy.

4. Simulations

4.1. Short-Time Forecasting Results for PV

To verify the reliability of the proposed forecasting method, the prediction results of the model with frequency decomposition and hyperparameters optimized by the SSA method are compared with those of the model without optimization by any optimization algorithm. The decomposition results of the original PV signals are shown in Figure 1. Then the decomposed signals are used in the SSA-TCN-LSTM forecasting method. To analyze the forecasting performance of the proposed method, LSTM, VMD-LSTM and VMD-TCN-LSTM are utilized to predict the short-term power value of PV. The prediction results of different methods are shown in Figure 2, and the prediction errors are shown in Figure 3. The quantitative forecasting performance of different methods is summarized in Table 2.

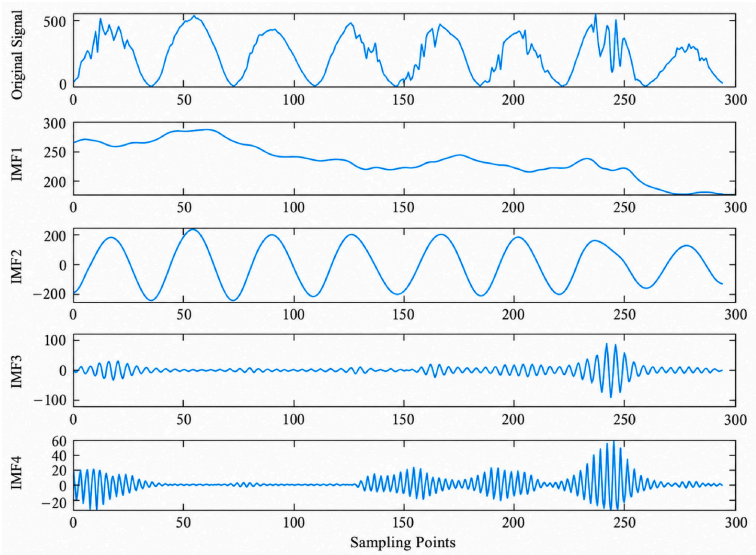


Figure 1. Decomposition results of PV signals.

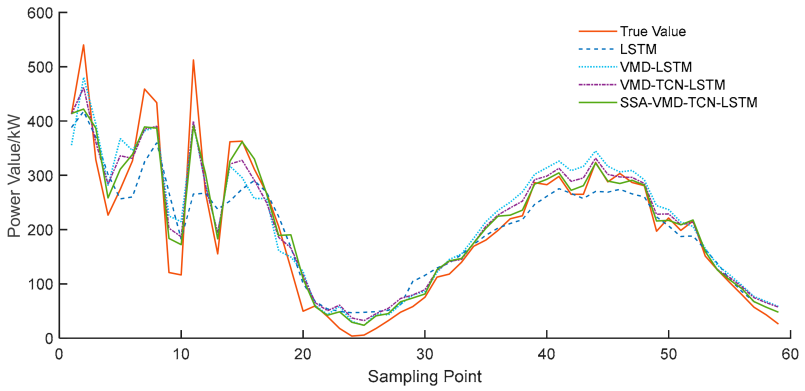


Figure 2. Prediction results of different methods.

Table 2. Prediction performance comparison of different forecasting methods.

Methods	MAE(kW)	MAPE(%)	MSE	RMSE(kW)	R^2
LSTM	37.50	58.20	3287	57.33	0.8071
VMD-LSTM	34.25	44.98	1858	43.10	0.8924
VMD-TCN-LSTM	26.63	48.16	1235	35.14	0.9285
VMD-SSA-TCN-LSTM	22.330	36.154	1149.8	33.909	0.9334

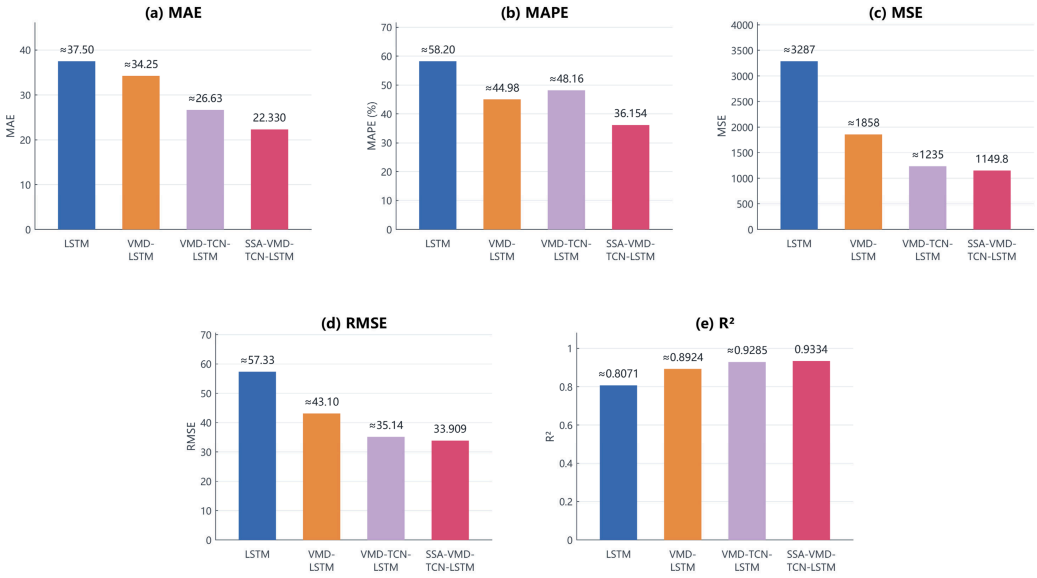


Figure 3. Prediction errors of different methods.

From Figures 2 and 3, the prediction error of LSTM is the largest, and the MAE value of LSTM is 37.5. The LSTM model exhibits significant deviations from actual values. This may be attributed to the fact that the model acts as a "black-box model". Single-model time-series forecasting cannot capture the physical mechanisms underlying changes in PV power output, resulting in limited prediction accuracy that fails to meet practical engineering requirements. The VMD-LSTM method combines the VMD signals, which can effectively extract the complex, latent information embedded in measured PV data. Compared with the LSTM method, the performance of VMD-LSTM is better.

From Figure 3, the MAE and R^2 values of the proposed method are 22.3 and 0.933 respectively. Compared with LSTM, VMD-LSTM and VMD-TCN-LSTM, the performance of the proposed method is the best. The SSA method optimizes the model parameters of the TCN-LSTM, leading to corresponding improvements in prediction accuracy. Therefore, the proposed method is suitable to short-term PV forecasting. The prediction values of PV power are employed for the fault reconfiguration.

To further evaluate the forecasting performance of the proposed method, comparisons are conducted with several forecasting models, including Transformer, Informer, and XGBoost. All models are trained and tested using the same dataset partition and evaluated using MAE, MAPE, MSE, RMSE, and R^2. The corresponding comparison results are presented in Table 3.

Table 3. Comparison results.

Methods	MAE (kW)	MAPE (%)	MSE	RMSE (kW)	R^2
XGBoost	31.42	46.73	1716.5	41.43	0.9016
Informer	28.07	42.85	1438.4	37.93	0.9168
Transformer	25.48	39.76	1248.6	35.34	0.9269
VMD-SSA-TCN-LSTM	22.330	36.154	1149.8	33.909	0.9334

Compared with XGBoost, Informer, and Transformer, the proposed VMD-SSA-TCN-LSTM model reduces the MAE by 28.93%, 20.45%, and 12.36%, respectively, demonstrating its improved accuracy in short-term PV power forecasting.

4.2. Reconfiguration of the Proposed Method

(1) Reconfiguration results

According to the forecasting results of DGs, the proposed reconfiguration method is used to recovery the loads of non-fault lines, reducing the impacts of the faults. The IEEE 33 node distribution network shown in Figure 4 is utilized. Three DG systems are installed at nodes 5, 12, and 28. The values of DGs are obtained by the proposed forecasting method.

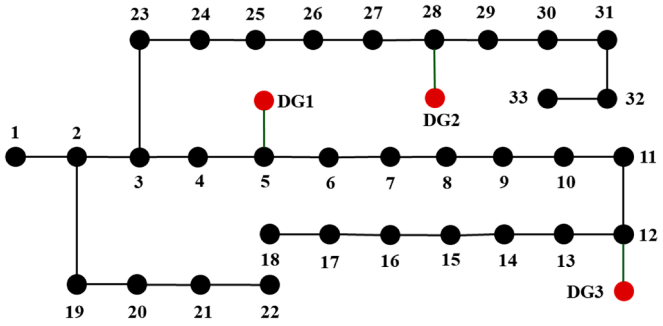


Figure 4. IEEE33 model of node distribution network.

Considering the types and importance of loads, all load nodes are classified into three different importance classes as follows:

(1) Class 1 loads: 2, 7, 13, 14, 24, 25, 30, 32.
(2) Class II loads: 8, 12, 16, 23, 27, 31, 33.
(3) Class III loads: 3, 4, 5, 6, 9, 10, 11, 15, 17, 18, 19, 20, 21, 22, 26, 28, 29.

During the fault reconfiguration, Class 1 loads are restored first, followed by Class 2 and Class 3 loads. When a fault occurs on line 8–9, severing the faulted sections by tripping the sectionalizing switches to isolate the affected feeders, dividing the system into two parts. In the event of a fault, the distributed generators (DG) will continue to operate normally, and buses 9–18 will form an islanded system powered by DG3. Considering the power capacity of DG3, it cannot supply enough power to all nodes. Thus, according to the proposed reconfiguration method, the switches are used to recover the non-fault nodes and branches. The fault reconfiguration results are shown in Figure 5 and Table 4.

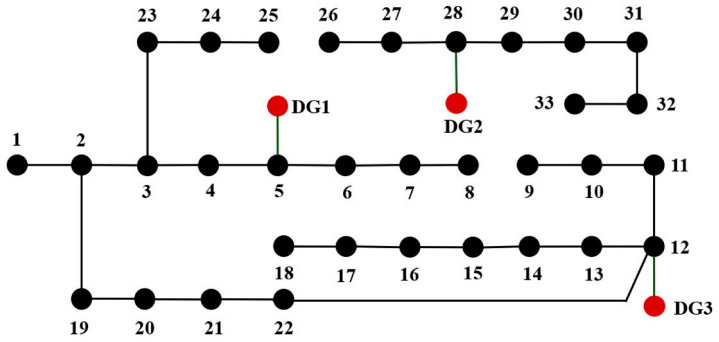


Figure 5. Reconfiguration of distribution network.

Table 4. Reconfiguration results.

Fault Line	Network Loss (kW)	Load Loss (kW)
8–9	47.340	0

From Figure 5, when a fault occurs on line 8–9, the faulted line is isolated and the tie switch between nodes 12 and 22 is closed for service restoration. After reconfiguration,

the disconnected area is supplied through the restored path, and all non-fault load nodes operate normally. According to Table 4, the load loss is zero and the network loss is 47.340 kW. The results show that the proposed method can effectively restore the loads in non-fault areas under a single-line fault condition.

When two faults occur on lines 6–7 and 15–16, the corresponding faulted sections are isolated, and the tie switches between nodes 8 and 21 and between nodes 18 and 33 are closed for service restoration, as shown in Figure 6. According to Table 5, all non-fault load nodes are restored, the load loss is zero, and the network loss is 52.862 kW. The results show that the proposed method can restore non-fault loads under multi-line fault conditions.

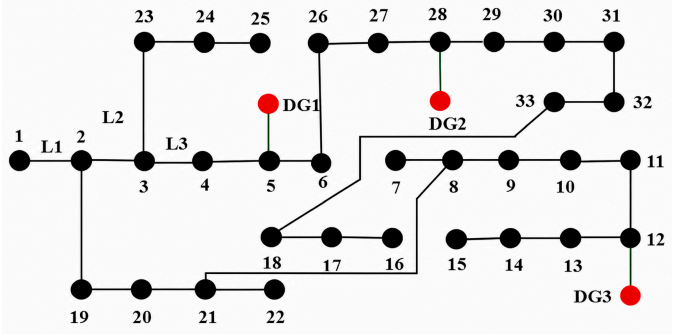


Figure 6. Reconfiguration result after faults on lines 6–7 and 15–16.

Table 5. Reconfiguration results.

Fault Line	Network Loss (kW)	Load Loss (kW)
6–7 15–16	52.862	0

(2) Comparisons with different methods

Scenario 1: Only the distribution network is isolated after the fault. The interconnection switches are not closed, and island operation is maintained only according to the DG outputs, without using the main grid to restore the remaining de-energized areas.

Scenario 2: The proposed reconfiguration method is applied without using the forecasted DG outputs. Instead, the historical average DG outputs are used for restoration.

Scenario 3: The proposed method is applied for distribution network fault restoration considering the forecasted DG outputs.

When two faults occur on lines 7–8 and 26–27, the three scenarios are simulated under the same fault condition. The fault restoration results are presented in Table 6.

Table 6. Reconfiguration results.

Methods	Class I Recovery Rate	Class II Recovery Rate	Class III Recovery Rate	Network Loss (kW)	Load Loss (kW)
Scenario 1	100%	61.76%	60.92%	25.58	770
Scenario 2	100%	100%	100%	68.67	0
Scenario 3	100%	100%	100%	49.55	0

In Scenario 1, a conventional islanding-based restoration strategy is used as a baseline. The interconnection switches remain open, resulting in a network loss of 25.58 kW and a load loss of 770 kW. The recovery rates of Class I, Class II and Class III loads are 100%, 61.76% and 60.92%, respectively.

In Scenario 2, the proposed reconfiguration method is applied using historical average DG outputs. All three classes of loads are fully restored, with zero load loss and a network loss of 68.67 kW.

In Scenario 3, the proposed method is applied using forecasted DG outputs. All three load classes are fully restored, with zero load loss and a network loss of 49.55 kW. Compared with Scenario 2, the network loss is further reduced, indicating that the forecasted DG outputs can improve the economic performance of the reconfiguration strategy.

To further verify the applicability of the proposed reconfiguration method to a larger-scale distribution network, the IEEE 69-bus system is employed for additional simulation. Two simultaneous faults are assumed to occur on lines 12–13 and 56–57. The reconfiguration result of the IEEE 69-bus distribution system under the simultaneous double-line faults on lines 12–13 and 56–57 is shown in Figure 7. The reconfiguration results under different network scales and multiple-fault conditions are summarized in Table 7.

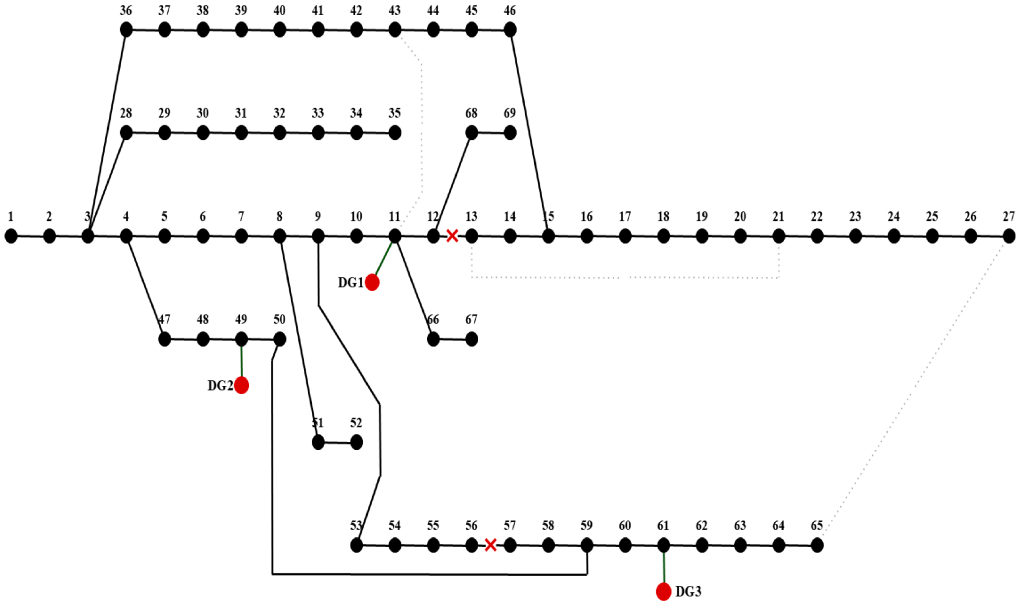


Figure 7. Reconfiguration result of the IEEE 69-bus distribution system.

Table 7. Reconfiguration results under different network scales and multiple-fault conditions.

System	Faulted Lines	Network Loss (kW)	Class I Recovery Rate	Class II Recovery Rate	Class III Recovery Rate
IEEE 33	6–7, 15–16	52.862	100%	100%	100%
IEEE 33	8–9, 20–21, 29–30	36.240	88.44%	70.59%	43.68%
IEEE 69	12–13, 56–57	32.814	100%	100%	100%

As shown in Table 7, the restoration performance varies with the fault conditions and post-fault network topology. For the double-line faults on lines 6–7 and 15–16 in the IEEE 33-bus system, all three classes of loads can be completely restored, with a network loss of 52.862 kW. Under the three-line fault condition on lines 8–9, 20–21, and 29–30, the recovery rates of Class I, Class II, and Class III loads are 88.44%, 70.59%, and 43.68%, respectively, while the network loss is 36.240 kW. The progressively decreasing recovery rates from Class I to Class III indicate that, when the available restoration capability is limited, the proposed method gives priority to higher-priority loads. The results also show that the restoration performance is affected not only by the number of faulted lines, but also by the fault locations, post-fault network topology, available DG capacity, and feasible restoration

paths. For the double-line faults on lines 12–13 and 56–57 in the IEEE 69-bus system, all three classes of loads are fully restored, with a network loss of 32.814 kW. These results demonstrate that the proposed method can be applied to distribution networks of different scales and can perform load restoration under different multiple-fault conditions.

4.3. Sensitivity Analysis of Key Operating Factors

A single-factor sensitivity study was conducted on the IEEE 33-bus system. DG penetration, fault location, and load level were varied separately while the remaining independent inputs were fixed.

The base case uses a 12.66 kV network, a 10 MVA per-unit base, 3715 kW of active demand, and simultaneous faults on lines 6–7 and 15–16. DGs at buses 5, 12, and 28 have assumed active-power capacities of 650, 650, and 1000 kW, with available outputs of 450, 500, and 650 kW. Their apparent-power ratings are 800, 800, and 1400 kVA, and reactive-power limits are 450, 450, and 1000 kvar. Grid-forming capability is assumed. Voltage limits are 0.95–1.05 p.u.; branch and main-grid limits are 5 MVA and 10 MVA, respectively.

Recovery is the served active demand divided by the pre-fault active demand of the same class at the tested load level. Base-case Class I, II, and III demands are 1730, 680, and 1305 kW. Unserved load is the sum of disconnected active demand; network loss is the total active line loss across all energized components.

DG penetration is installed DG active-power capacity divided by the fixed base demand of 3715 kW. Levels of 20%, 40%, and 61.91% (base) are tested. The corresponding reconfiguration results under different DG penetration levels are shown in Table 8.

Table 8. Sensitivity to DG penetration.

DG Penetration (%)	Network Loss (kW)	Class I Recovery (%)	Class II Recovery (%)	Class III Recovery (%)
20	82.943	100.00	100.00	79.31
40	75.065	100.00	100.00	100.00
61.91 (base)	52.862	100.00	100.00	100.00

At a DG penetration level of 20%, the recovery rates of Class I and Class II loads reach 100%, while the recovery rate of Class III loads is 79.31%. When the DG penetration level increases to 40% and above, all three classes of loads can be fully restored. These results indicate that increasing DG penetration can enhance the load restoration capability and reduce network losses under the tested conditions.

The influence of load level on the restoration performance is also investigated by varying the system demand while keeping the fault condition and DG parameters unchanged. The corresponding results are presented in Table 9.

Table 9. Sensitivity to load level.

Load Level (%)	Network Loss (kW)	Class I Recovery (%)	Class II Recovery (%)	Class III Recovery (%)
80	28.594	100.00	100.00	100.00
90	39.442	100.00	100.00	100.00
100 (base)	52.862	100.00	100.00	100.00
110	68.928	100.00	100.00	100.00
120	80.911	100.00	100.00	95.40

Full restoration of all three load classes is achieved when the load level ranges from 80% to 110%. When the load level increases to 120%, the recovery rates of Class I and

Class II loads remain at 100%, while the recovery rate of Class III loads decreases to 95.40%. The network loss increases from 28.594 kW at the 80% load level to 80.911 kW at the 120% load level. These results indicate that increasing the load level increases the power-transfer requirement and network losses, and may reduce the restoration capability for lower-priority loads under heavy-load conditions.

Overall, the sensitivity analysis shows that DG penetration, fault location, and load level all affect the restoration performance of the proposed method. Class I loads remain fully restored under all tested conditions, demonstrating the priority given to critical loads. The results also indicate that the proposed method can adapt the restoration strategy according to variations in generation capacity, fault location, and system demand.

5. Conclusions

This paper investigates the problem of fault restoration in distribution grids under varying solar conditions, focusing on both power forecasting and restoration reconstruction. The main conclusions are as follows:

(1) The SSA method can optimize the parameters of VMD and TCN-LSTM, addressing the issues of inappropriate parameter selection or the difficulty in selecting parameters for VMD and TCN-LSTM. The proposed forecasting method has a better performance of PV power prediction.

(2) A photovoltaic power prediction method is established to mitigate the impact of photovoltaic output uncertainty on islanding classification, thereby ensuring the stability of power supply to the islanded system. By considering the importance of loads and their time-varying demands, islanding classification is performed using a combined BFS and DFS approach to prioritize the restoration of critical loads.

Author Contributions: Conceptualization, W.F. and L.S.; methodology, W.F. and C.K.; software, W.F.; validation, W.F., C.K., M.W. and X.Y.; formal analysis, W.F. and X.Y.; investigation, W.F. and L.S.; resources, M.W. and R.G.; data curation, W.F.; writing—original draft preparation, W.F.; writing—review and editing, L.S., M.W., R.G. and X.Y.; visualization, W.F. and C.K.; supervision, L.S. and R.G.; project administration, R.G.; funding acquisition, L.S. and R.G. All authors have read and agreed to the published version of the manuscript.

Funding: This research was supported in part by the Science and Technology Project of State Grid Corporation of China under Grant 521532240029.

Data Availability Statement: The data presented in this study are available on request from the corresponding author.

Conflicts of Interest: W.F., L.S., C.K., M.W., and R.G. were employed by State Grid Hubei Electric Power Research Institute. The authors declare that this study received funding from the Science and Technology Project of State Grid Corporation of China under Grant 521532240029. The funder was not involved in the study design, data collection, analysis, interpretation of data, the writing of this article, or the decision to submit it for publication. The remaining author declares no conflict of interest.

References

1. Wang, C.; Li, P.; Yu, H. Development and characteristic analysis of flexibility in smart distribution network. *Autom. Electr. Power Syst.* **2018**, *42*, 13–21.
2. Xiao, B.; Guo, B. Review and prospect of distribution network planning. *Electr. Power Autom. Equip.* **2018**, *38*, 200–211, 217.
3. Golshani, A.; Sun, W.; Sun, K. Advanced power system partitioning method for fast and reliable restoration: Toward a self-healing power grid. *IET Gener. Transm. Distrib.* **2018**, *12*, 42–52. [CrossRef]
4. Shariatzadeh, F.; Vellaithurai, C.B.; Biswas, S.S.; Zamora, R.; Srivastava, A.K. Real-time implementation of intelligent reconfiguration algorithm for microgrid. *IEEE Trans. Sustain. Energy* **2014**, *5*, 598–607. [CrossRef]

5. Mendoza, J.; Lopez, R.; Morales, D.; Lopez, E.; Dessante, P.; Moraga, R. Minimal loss reconfiguration using genetic algorithms with restricted population and addressed operators: Real application. *IEEE Trans. Power Syst.* **2006**, *21*, 948–954. [CrossRef]
6. Sekhavatmanesh, H.; Cherkaoui, R. Distribution network restoration in a multi-agent framework using a convex OPF model. *IEEE Trans. Smart Grid* **2019**, *10*, 2618–2628. [CrossRef]
7. Li, Y.; Xiao, J.; Chen, C.; Tan, Y.; Cao, Y. Service restoration model with mixed-integer second-order cone programming for distribution network with distributed generation. *IEEE Trans. Smart Grid* **2018**, *9*, 4138–4150. [CrossRef]
8. Zhu, J.; Gu, W.; Jiang, P.; Wu, Z.; Yuan, X.; Nie, Y. Integrated approach for optimal island partition and power dispatch. *J. Mod. Power Syst. Clean Energy* **2018**, *6*, 449–462. [CrossRef]
9. Lin, C.; Chen, C.; Bie, Z.; Li, G. Post-disaster load restoration method for urban distribution network with dynamic un certainty and frequency-voltage control. *Autom. Electr. Power Syst.* **2022**, *46*, 56–64.
10. Li, C.; Xi, Y.; Lu, Y.; Liu, N.; Chen, L.; Ju, L.; Tao, Y. Resilient outage recovery of a distribution system: Co-optimizing mobile power sources with network structure. *Prot. Control Mod. Power Syst.* **2022**, *7*, 459–471. [CrossRef]
11. Shi, X.; Ke, Q.; Lei, J.; Yuan, Z. Fault reconfiguration of distribution networks with soft open points considering the uncertainties of photovoltaics and loads. *South. Power Syst. Technol.* **2020**, *14*, 56–61.
12. Xu, Y.; Zhang, H.; Ma, T.; Yao, J.M. Coordinated optimization strategy of fault emergency recovery and repair for distribution network with distributed generators. *Autom. Electr. Power Syst.* **2021**, *45*, 38–46.
13. Mahdavi, M.; Awaafo, A.; Djokic, S.Z.; Schmitt, K.; Chamana, M. Coordinated feeder reconfiguration, capacitor placement and allocation of distributed energy resources for loss reduction under variable loading condition. In Proceedings of the IEEE Kansas Power and Energy Conference (KPEC), Manhattan, NY, USA, 27–28 April 2023; pp. 1–6.
14. He, M.; Ma, C.; Duan, Q.; Ni, S.; Deng, W.; Liu, X.; Li, Z.; Chen, Y.; Shi, Y. Active distribution network reconfiguration method based on photovoltaic generation prediction. In Proceedings of the IEEE International Conference on Electrical Engineering, Big Data and Algorithms (EEBDA), Changchun, China, 25–27 February 2022; pp. 82–87.
15. Pan, K.; Zhao, R.; Liu, S. Distribution network reconfiguration considering power load demand and distributed power source uncertainty. *Renew. Energy Resour.* **2024**, *42*, 546–552.
16. Chen, Z.; Zhang, Y.; Huang, Y.; Qin, Y.; Chen, B.D.; Lin, K.D. Optimal recon figuration of distribution networks in integrated energy systems based on conditional value at risk. *J. Glob. Energy Interconnect.* **2020**, *3*, 590–599.
17. Gandoman, F.H.; Aleem, S.H.A.; Omar, N.; Ahmadi, A.; Alenezi, F.Q. Short-term solar power forecasting considering cloud coverage and ambient temperature variation effects. *Renew. Energy* **2018**, *123*, 793–805. [CrossRef]
18. Koster, D.; Minette, F.; Braun, C.; O'NAgy, O. Short-term and regionalized photovoltaic power forecasting, enhanced by reference systems, on the example of Luxembourg. *Renew. Energy* **2019**, *132*, 455–470. [CrossRef]
19. Wu, H.B.; Shi, M.; Zheng, H.; Zhang, J.; Zhang, H. Short-term interval prediction of photovoltaic power based on EEMD-ALOCO SVM model. *Acta Energiae Solaris Sin.* **2023**, *44*, 64–71.
20. Wu, Y.K.; Huang, C.L.; Phan, Q.T.; Li, Y.Y. Completed review of various solar power forecasting techniques considering different viewpoints. *Energies* **2022**, *15*, 3320. [CrossRef]
21. Almeida, M.P.; Muñoz, M.; de la Parra, I.; Perpiñán, O. Comparative study of PV power forecast using parametric and nonparametric PV models. *Sol. Energy* **2017**, *155*, 854–866. [CrossRef]
22. Jalali, S.M.J.; Ahmadian, S.; Kavousi-Fard, A.; Khosravi, A.; Nahavandi, S. Automated Deep CNN-LSTM Architecture Design for Solar Irradiance Forecasting. *IEEE Trans. Syst. Man Cybern.-Syst.* **2022**, *52*, 54–65. [CrossRef]
23. Antonanzas, J.; Osorio, N.; Escobar, R.; Urraca, R.; Martinez-de-Pison, F.J.; Antonanzas-Torres, F. Review of photovoltaic power forecasting. *Sol. Energy* **2016**, *136*, 78–111. [CrossRef]
24. Liu, Y.; Zhang, Z.; Ma, L.; Jia, Y.; Yin, W.; Liu, Z. Short-Term Prediction of Photovoltaic Power Based on DBSCAN-SVM Data Cleaning and PSO-LSTM Model. *Energy Eng.* **2024**, *121*, 3019–3035. [CrossRef]
25. Zhao, Y.; Peng, X.; Tu, T.; Li, Z.; Yan, P.; Li, C. WOA-VMD-SCINet: Hybrid Model for Accurate Prediction of Ultra-Short-Term Photovoltaic Generation Power Considering Seasonal Variations. *Energy Rep.* **2024**, *12*, 3470–3487. [CrossRef]
26. Jia, P.; Zhang, H.; Liu, X.; Gong, X. Short-Term Photovoltaic Power Forecasting Based on VMD and ISSA-GRU. *IEEE Access* **2021**, *9*, 105939–105950. [CrossRef]
27. Tang, H.; Wang, S.; Lai, S.; Chen, Y.; Yang, W.; Xiao, G.; Zhang, X. Quasi-Steady-State CEST Prediction Based on TCN-LSTM. *IEEE Access* **2023**, *11*, 97189–97197. [CrossRef]

Disclaimer/Publisher's Note: The statements, opinions and data contained in all publications are solely those of the individual author(s) and contributor(s) and not of MDPI and/or the editor(s). MDPI and/or the editor(s) disclaim responsibility for any injury to people or property resulting from any ideas, methods, instructions or products referred to in the content.